Solid-State Electronics 125 (2016) 161–166

Contents lists available at ScienceDirect

Solid-State Electronics

journal homepage: www.elsevier.com/locate/sse

Contact resistance extraction methods for short- and long-channel carbon nanotube field-effect transistors

Anibal Pacheco-Sanchez [a,*], Martin Claus [a,b], Sven Mothes [a,b], Michael Schröter [a,c]

[a] Department of Electrical and Computer Engineering, Technische Universität Dresden, Germany
[b] Center for Advancing Electronics Dresden, Technische Universität Dresden, Germany
[c] Department of Electronics and Communication Engineering, University of California at San Diego, USA

ARTICLE INFO

Article history:
Available online 18 July 2016

The review of this paper was arranged by Jurriaan Schmitz

Keywords:
CNTFET
Contact resistance
Y-function method

ABSTRACT

Three different methods for the extraction of the contact resistance based on both the well-known transfer length method (TLM) and two variants of the Y-function method have been applied to simulation and experimental data of short- and long-channel CNTFETs. While for TLM special CNT test structures are mandatory, standard electrical device characteristics are sufficient for the Y-function methods. The methods have been applied to CNTFETs with low and high channel resistance. It turned out that the standard Y-function method fails to deliver the correct contact resistance in case of a relatively high channel resistance compared to the contact resistances. A physics-based validation is also given for the application of these methods based on applying traditional Si MOSFET theory to quasi-ballistic CNTFETs.

1. Introduction

Carbon nanotube field-effect transistors (CNTFETs) have the potential to become relevant for RF electronics due to the outstanding electrical characteristics of the carbon nanotubes (CNTs) used as a channel. Fabricated CNTFETs have already achieved an intrinsic transit frequency of 80 GHz and extrinsic transit and maximum oscillation frequencies of around 10 GHz as well as a maximum available power gain of 10 dB at 2 GHz [1,2].

Among the extraordinary electrical characteristics, such as low scattering rate and high current-carrying capability, the intrinsic linearity [3–6] is expected to be beneficial for future high-frequency applications such as CNTFET amplifiers, mixers and switches once the technology related issues are solved [2]. A full review of the state-of-the-art of CNTFET technology for RF applications can be found in [2].

One of the key effects that limits the performance of CNTFETs, and thus its RF linearity, is the resistance associated with the interconnection between the CNT and the metal contacts, which is commonly labeled as the contact resistance.

Extracting the values for this contact resistance from experimental data is of interest to various research disciplines: from a technological point of view this value represents a quantification of the contact quality while from a modeling point of view this resistance can be associated with the series resistance in the equivalent circuit of a CNTFET compact model. In addition, the extracted value can also be used for verifying sophisticated contact models based on, e.g., atomistic simulations.

In the literature, different methods for extracting the contact resistance of CNTFETs are discussed. Interestingly, the extracted values can differ by orders of magnitude. Therefore, in this paper the reliability of three often found methods is analyzed and compared based on simulation and experimental data.

This paper is organized as follows. Section 2 introduces a definition of the contact resistance and explains its physical origin. Section 3 describes the methodologies applied to extract the value associated to the contact resistance. The methods have been applied to synthetic data from a compact model and numerical device simulations as well as to measurements of single- and multi-tube CNTFETs. The corresponding results are discussed in Section 4.

2. The contact resistance in CNTFETs

The total resistance R_{tot} of a CNTFET measurable at the terminals can be seen as the sum of the resistance R_{ch} of the channel and the contact resistances $R_{CS/D}$ associated with the source and drain contacts, i.e., $R_{tot} = R_{ch} + R_{CS} + R_{CD}$. The separation of the total resistance into channel and contact resistance is not unique. Especially in the case of Schottky-barrier transistors the impact of the Schottky barrier on the $I - V$ characteristics can be lumped either

* Corresponding author.
E-mail addresses: anibal.pacheco-sanchez@mailbox.tu-dresden.de (A. Pacheco-Sanchez), martin.claus@tu-dresden.de (M. Claus).

http://dx.doi.org/10.1016/j.sse.2016.07.011
0038-1101/

into the channel or into a bias dependent contact resistance depending on the motivation for doing the extraction. In this work, the contributions of the source and drain contacts are lumped into a total contact resistance $R_C = R_{CS} + R_{CD}$ which includes the impact of the Schottky barriers unless specified otherwise.

The channel resistance R_{ch} depends on the number of scattering events in the channel. The shorter the channel, the smaller is the number of scattering events, and, thus, the smaller is the contribution of R_{ch} to R_{tot}. For very short channels and ohmic contacts, R_{tot} approaches its ballistic limit corresponding to the value of the quantum resistance R_q of about 6.5 kΩ per subband. Experimentally, defects can affect considerably the channel resistance even when the channel length is short. The devices considered here are working in the quasi-ballistic and in the diffusive regimes. For the latter, a quantifiable contribution of R_{ch} to R_{tot} is thus expected.

As shown in Fig. 1, in general, two main material interfaces contribute to the contact resistance in CNTFETs: the first material interface is in between the metal and the nanotube portion under the metal (coated CNT region) while the second material interface is in between the coated and uncoated nanotube portion.

The first interface can be influenced by several parameters such as contact geometry, contact length [7], the material used for the fabrication [8], and any interfacial layer that may be present between the metal and the nanotube. At the second interface, a change of the electronic structure of the metal-coated tube portion due to the interaction with the metal induces a potential step (barrier) [9–11]. An important contribution to the height of the potential step is the Schottky barrier height ϕ_{SB} which is defined as the difference between the Fermi level and the value of conduction band of the CNT at the interface between the metal coated and uncoated tube portion.

3. Contact resistance extraction methods

Three different extraction methodologies are used in this work: the transfer length method (TLM) [12] widely known in the MOSFET and bipolar transistor community and two methods based on the Y-function [13] developed for Si MOSFETs using simple analytical MOSFET equations. The Y-function has been used recently to extract the contact resistance of CNTFETs in [14,15].

The TLM requires the fabrication of a test structure with long CNTs [8], which allows the placement of various contacts on the tube with different spacings L_{ch} in between the contacts. The CNT should lie on a substrate with a global back gate to bias the device properly. The resistance R_{tot} between each pair of contacts is obtained from the $I-V$ measurements at these contacts. The contact resistance is extracted from the linear extrapolation of the $R_{tot}(L_{ch})$ plot towards $L_{ch} = 0$. However, the need for typically μm-long CNTs makes the fabrication of these test structures challenging in, e.g., purified solution based technologies.

The Y-function method is based on a combination of the current and transconductance equations in order to avoid the effects of the mobility reduction on the determination of device model parameters [13]. In general, the Y-function is defined as

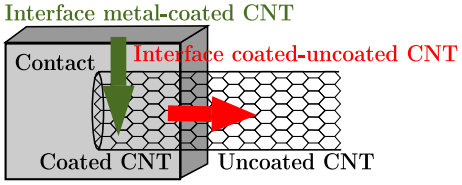

Fig. 1. Internal device interfaces involved in the CNTFETs contact resistance. (Only one contact is shown).

$$Y = \frac{I_D}{\sqrt{g_m}}, \tag{1}$$

where I_D is the drain current and g_m the transconductance, defined as the derivative of I_D with respect to the gate-source voltage, V_{GS} at constant drain-source voltage, V_{DS}.

The device is considered within the strong inversion regime of the linear region at low drain-source voltages. The underlying transport model describing the current flow through the internal transistor is given by

$$I_D = \beta \frac{(V_{GS,i} - V_{th} - V_{DS,i}/2)}{1 + \theta_0 (V_{GS,i} - V_{th})} V_{DS,i}, \tag{2}$$

where $\beta = \mu_0 C_G / L_{ch}^2$ with the gate capacitance $C_G = C_{ox} W L_{ch}$; C_{ox} is the area specific gate oxide capacitance, W is the effective channel width, L_{ch} is the effective channel length, μ_0 is the low field carrier mobility, θ_0 is the mobility reduction coefficient which quantifies the degradation of the carrier mobility due to the applied vertical field [12], V_{th} is the threshold voltage, and $V_{GS,i}$ and $V_{DS,i}$ are the internal gate-to-source and internal drain-to-source terminal voltages, respectively. The internal voltages are given by $V_{GS,i} \approx V_{GS} - I_D R_C/2$ and $V_{DS,i} \approx V_{DS} - I_D R_C$. Assuming $R_C = R_{CS} + R_{CD}$ leads to

$$I_D \approx \beta \frac{(V_{GS} - V_{th} - V_{DS}/2)}{1 + \theta (V_{GS} - V_{th} - V_{DS}/2)} V_{DS}, \tag{3}$$

where the extrinsic mobility degradation coefficient θ, including the contribution from the contact resistance [12], is given by

$$\theta = \theta_0 + R_C \beta. \tag{4}$$

Note that in the denominator of Eq. (3) the voltage drop over the intrinsic transistor diminished by the mobility reduction coefficient $(\theta_0 V_{DS,i}/2)$ has been neglected.

The Y-function method applied in [14,15], labeled here YFM_1, assumes $V_{GS} - V_{th} \gg V_{DS}/2$ and a negligible mobility reduction coefficient ($\theta_0 = 0$). Hence the drain current expression used in YFM_1 is given as

$$I_D \approx \beta \frac{(V_{GS} - V_{th})}{1 + R_C \beta (V_{GS} - V_{th})} V_{DS}, \tag{5}$$

with the parameters V_{th} and β obtained from the intercept and slope of a linear plot $Y(V_{GS})$ [14,15]. Replacing I_D in Eq. (1) by Eq. (5), the Y-function reduces to

$$Y = \sqrt{\beta V_{DS}} (V_{GS} - V_{th}). \tag{6}$$

Defining $R_{tot} = V_{DS}/I_D$, the contact resistance $R_{C,Y1}$ is obtained by

$$R_{C,Y1} = R_{tot} - R_{ch}, \tag{7}$$

where the channel resistance is approximated at small V_{DS} with

$$R_{ch} \approx \frac{1}{\beta (V_{GS} - V_{th})}. \tag{8}$$

YFM_1 yields a range of contact resistance values for $R_{C,Y1}$ according to the range of the applied gate bias voltages V_{GS}.

In [16] an improved method was developed for the extraction of the contact resistance in SOI-MOSFETs which considers the mobility reduction coefficient, θ_0, in Eq. (3) but still assumes $V_{GS} - V_{th} \gg V_{DS}/2$ in the denominator. In this work, however, the latter approximation is not considered in the calculations. Thus, Eq. (3) is used as the underlying transport model. The related extraction method is labeled here with YFM_2. Replacing I_D in Eq. (1) by Eq. (3), the Y-function reduces to

$$Y = \sqrt{\beta V_{DS}} \left(V_{GS} - V_{th} - \frac{V_{DS}}{2} \right). \tag{9}$$

The contact resistance $R_{C,Y2}$ is extracted from the slope of the linear relation $\theta(\beta)$ given by Eq. (4) afer obtaining θ and β by means of the Y-function [16]. The procedure and considerations to obtain θ and β in this method differ from the ones in YFM_1.

Note that β extracted from experimental data shows a slight V_{DS} dependence which is caused by the approximations considered to obtain Eq. (3) from Eq. (2). Without these approximations, the expression to obtain β is

$$\beta = \frac{Y'^2_{max}}{V_{DS}}\left(1 + \theta_0 \frac{V_{DS}}{2}\right). \quad (10)$$

From experimental data, the internal voltages in Eq. (2) are difficult to obtain, therefore the considerations to get Eq. (3) are needed and then the V_{DS} dependence of β is not explicitly included.

YFM_2 provides a single value for the contact resistance $R_{C,Y2}$. Further details on the method can be found in [16]. The advantage of YFM_2 over YFM_1 is that no expression for the channel resistance is required. According to the authors' knowledge, YFM_2 is applied for the first time to devices such as CNTFETs where the ratio between channel and contact resistance can be much smaller than one, i.e., for devices where the contact resistance can dominate the total resistance.

The Y-function based methods have been developed based on Si MOSFET theory and have been applied to long-channel devices in contrast to the devices used in this work. Nevertheless, according to the discussion in [17] the traditional MOSFET models can be reinterpreted for nanoscale devices. This is done by considering the apparent mobility μ_{app} rather than the low-field mobility μ_0, and the injection velocity υ_{inj} rather than the high-field saturation velocity υ_T in the underlying drain current expression. Equations of nanoscale devices and traditional MOSFETs are then similar but include parameters with different physical implications. μ_0 represents here the channel mobility, while μ_{app}, in the context of CNTFETs, not only considers the channel mobility, but the contact and quantum resistance effects as well. Both parameters, μ_{app} and υ_{inj}, including a limitation for the ballistic and diffusive limit, make the model usable in ballistic and quasi-ballistic transport regimes and thus a valuable basis for the YFMs applied here to CNTFETs with channel lengths in the range of 30 nm to 800 nm.

4. Results and discussion

4.1. Compact model data

The semiphysical large signal compact model CCAM [18,19] is used for generating synthetic data to test the different extraction methods. In CCAM, the impact of Schottky barriers is captured by the current source describing the current flow through the channel, while a series contact resistance $R_{C,EC}$ in the equivalent circuit (EC) is added to capture the contribution of the metal-to-CNT interface on the contact resistance. The contribution of R_q is not included in $R_{C,EC}$. In this work, the model parameters of CCAM are chosen for modeling devices with a channel length of about 700 nm (more parameters of the model are mentioned in [19]) and such that the Schottky-barrier has a negligible impact on the $I-V$ characteristics.

Semiconducting single-tube (ST) CNTFETs with $R_{C,EC} = 20\,k\Omega, 50\,k\Omega, 100\,k\Omega$ are modeled with CCAM. Different values of an initial prefactor of the current in the model (see Eq. (2) in [19]) enable different values of R_{ch}. High channel resistances are also considered in this study since experimental results (see Section 4.3) suggest that the channel resistance may be much larger than the contact resistance as common for other semiconducting technologies.

As an example, in Fig. 2 the transfer characteristics obtained for a device with $R_{C,EC} = 100\,k\Omega$ are shown, where the data represented with markers (triangles for YFM_1, circles for YFM_2) is obtained by recalculating the drain current with the corresponding expression used in each method (Eqs. (5) and (3), respectively) using the parameters θ, V_{th} and β extracted with the corresponding method. These curves also indicate the bias region where the YFMs have been applied. The latter gives a fast and reasonable verification of the methods.

The method which gives with 114.2 kΩ the closest value to $R_{C,EC}$ for this device is YFM_2. YFM_1, in contrast, gives values in between $R_{C,Y1}$ = 164 kΩ and 172 kΩ. The comparison of the curves in Fig. 2 shows an excellent agreement between the calculated drain current from YFM_2 for not too large V_{DS} while the calculation from YFM_1 does not match the simulated data. YFM_1 fails due to the approximations used in deriving its underlying Eq. (5), i.e. neglecting the voltage drop across the contact resistance ($V_{GS} - V_{th} \gg V_{DS}/2$). Due to a similar approximation, the method presented in [16] fails to give a good match between the calculated current and the reference data (comparison not shown here).

CNTFETs with different channel resistance $R_{ch}(= R_{tot} - R_{C,EC})$ have been simulated for each value of $R_{C,EC}$. Fig. 3 shows the extracted values of the contact resistances $R_{C,Y1}$ (mean value) and $R_{C,Y2}$ for these devices obtained with YFM_1 and YFM_2, respectively. Fig. 4 shows the relative error obtained by each method with respect to the ratio of R_{ch} to $R_{C,EC}$.

Obviously, the smaller R_{ch}, the closer are the extracted values to the reference values as it can be seen in Fig. 3. However for larger R_{ch}, only YFM_2 delivers still reasonable results. The same trend has been observed in the results obtained from the simulation of multi-tube (MT) CNTFETs modeled with CCAM (not shown here).

The results obtained for the devices simulated with CCAM suggest that YFM_2 extracts a value close to the reference contact resistance set in the equivalent circuit of the model.

4.2. BTE simulations

The numerical device simulator described in [4,21] is used for simulating the current voltage characteristics of identical ST CNTFETs but with different channel lengths, thus enabling to imitate a TLM test structure. The employed device simulator provides a self-consistent solution of the semiclassical Boltzmann transport equation (BTE) and the Poisson equation [4,21]. Optical and acoustic phonon scattering is included with the mean free paths for acoustic and optical phonons equal to 500 nm and 15 nm,

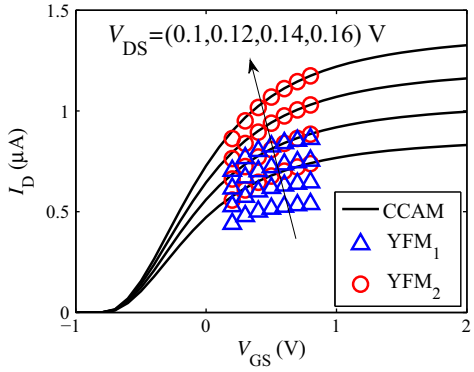

Fig. 2. Transfer characteristics of a ST CNTFET simulated using CCAM (solid lines) with $R_{C,EC} = 100\,k\Omega$. Triangles: I_D calculated with the mean values of the parameters extracted from YFM_1 ($R_{C,Y1}$ = 164 kΩ to 172 kΩ, β = 90.51 μA V^{-2}, and $V_{th} = 0.77$ mV). Circles: I_D calculated with the mean values of the parameters extracted from YFM_2 ($R_{C,Y2} = 114.23\,k\Omega, \beta = 35.27\,\mu A\,V^{-2}$, $\theta = 3.76\,V^{-1}$, and V_{th} = −240 mV).

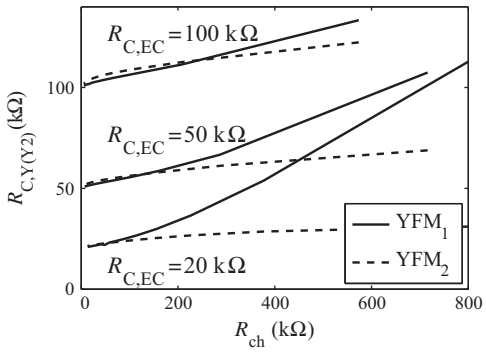

Fig. 3. Contact resistance extracted with the different YFMs for ST CNTFETs with $R_{C,EC} = 20\ k\Omega, 50\ k\Omega, 100\ k\Omega$ and different values of channel resistance.

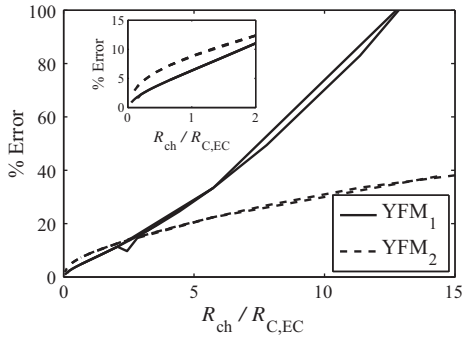

Fig. 4. Relative error in the extracted value of the contact resistance with different methods for $R_{C,EC} = 20\ k\Omega, 50\ k\Omega, 100\ k\Omega$. The curves of the relative error for $R_{C,EC} = 50\ k\Omega$ and $100\ k\Omega$ are almost identical.

respectively. The simulation boundaries for the BTE and the Poisson equation, are set directly at the interfaces between the coated and uncoated CNT portions. Tunneling through Schottky barriers is considered by means of the WKB method. Note that an additional contact resistance is not included.

The simulated devices have 5 nm oxide thickness, an oxide permittivity of 16, a tube diameter of 1.8 nm, a spacer length (distance between drain or source to the gate contacts) of 5 nm and channel lengths ranging from 30 nm to 800 nm. The simulations have been performed at $V_{DS} = 50$ mV and $V_{GS} = 1$ V for Schottky barrier heights of 0.1 eV and −0.2 eV, where the latter value mimics an ohmic-like contact. A single sub-band has been considered for the simulations. The TLM plot obtained for these devices is shown in Fig. 5.

The values of the contact resistance $R_{C,TLM}$ extracted with the TLM are 14.1 kΩ for $\phi_{SB} = 0.1$ eV and 6.7 kΩ for $\phi_{SB} = -0.2$ eV. The latter result is close to the ballistic limit of the total resistance of about 6.5 kΩ per sub-band, which is expected for short channel devices with an ohmic-like contact.

The Y-function based methods are applied first to the simulated device with the shortest channel length ($L_{ch} = 30$ nm), for both values of ϕ_{SB} within the same bias region where TLM has been applied. Table 1 lists the contact resistances extracted with the different methods. Note that $R_{tot} = V_{DS}/I_D$ is extracted from the output characteristics for low V_{DS}. It can be seen that YFM$_1$ overestimates the contact resistance considerably and leads to values which are even larger than the total resistance. In contrast, the extracted values from YFM$_2$ are close to the values extracted with TLM for both types of devices. Hence, from this comparison it can be claimed that YFM$_2$ is a more reliable method than YFM$_1$ for extracting the contact resistance.

For the device with $\phi_{SB} = 0.1$ eV (−0.2 eV) the channel resistance is 0.5 kΩ (0.2 kΩ) which is obtained as $R_{ch} = R_{tot} - R_{C,Y2}$.

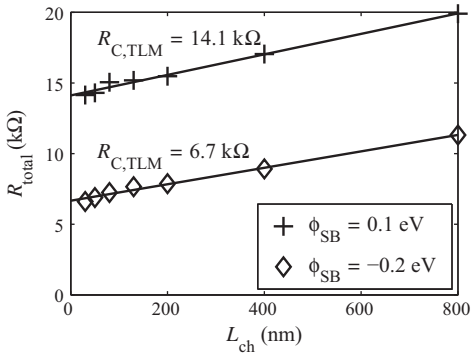

Fig. 5. TLM plot of the devices simulated with BTE simulator for different Schottky barrier heights and L_{ch} = 30 nm, 50 nm, 80 nm, 130 nm, 200 nm, 400 nm and 800 nm. The solid lines represent the linear extrapolation of each set of data.

Table 1
Contact resistances extracted with TLM and YFMs from BTE simulations. $L_{ch} = 30$ nm. $R_{tot} = V_{DS}/I_D$ is extracted from the output characteristic at $V_{DS} = 50$ mV and $V_{GS} = 1$ V.

	$\phi_{SB} = -0.2$ eV	$\phi_{SB} = 0.1$ eV
$R_{C,TLM}$ (kΩ)	6.7	14.1
$R_{C,Y1}$ (kΩ)	11.1–12.1	10–21
$R_{C,Y2}$ (kΩ)	6.9	14.2
R_{tot} (kΩ)	7.2	14.6

Table 2
Contact resistances extracted with TLM and YFM$_2$ from BTE simulations of a 30 nm and a 400 nm ST-CNTFETs with $\phi_{SB} = 0.1$ eV. $R_{tot} = V_{DS}/I_D$ is extracted from the output characteristic at $V_{DS} = 50$ mV and $V_{GS} = 1$ V.

	$L_{ch} = 30$ nm	$L_{ch} = 400$ nm
$R_{C,TLM}$ (kΩ)	14.1	14.1
$R_{C,Y2}$ (kΩ)	14.2	15.7
R_{tot} (kΩ)	14.6	17.6

The ratio of the channel resistance over the contact resistance is less than 0.01 for both types of devices. As expected, for both devices the channel resistance is almost negligible.

In order to verify the feasibility of the YFM$_2$ for high channel resistance devices, the extraction method has also been applied to BTE simulation results of the device with $\phi_{SB} = 0.1$ eV and the same device parameters but with an increased channel length of 400 nm where scattering mechanisms are much more dominant than in shorter devices (i.e., an increase of R_{ch} is expected). The extracted values are compared with the extracted values of the simulated 30 nm ST-CNTFET in Table 2.

The extracted value $R_{C,Y2} = 15.7\ k\Omega$ for the device with $L_{ch} = 400$ nm is still quite close to the value of 14.2 kΩ extracted for the quasi-ballistic device with a channel length of 30 nm. The small deviation can be attributed to a difference in the electrostatics affecting the shape of the Schottky barrier and thus the current flow. The total resistance of the long channel device is about 17.6 kΩ. The difference of about 3 kΩ between the total resistance of these devices is thus only due to scattering within the channel. The similarity of the extracted value for the contact resistance of both, a short- and a relatively long-channel device, suggests that the value obtained with YFM$_2$ does not include significant contributions of scattering in the channel but the Schottky barrier.

4.3. Measurements

4.3.1. Single-tube CNTFET

Standard DC measurements have been performed on a top-gate ST CNTFET with a channel length of about 800 nm (more

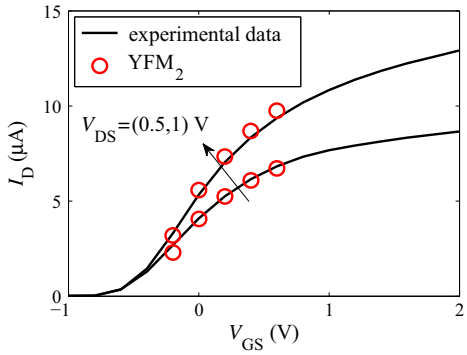

Fig. 6. Measured transfer characteristic of a ST CNTFET with a channel length of about 800 nm. Solid lines: experimental data. Circles: I_D calculated with Eq. (3) using $R_{C,Y2} = 33.1\ k\Omega$ and the mean values of the parameters extracted with YFM_2 ($\beta = 23.1\ \mu A\ V^{-2}, \theta = 1.2\ V^{-1}$ and $V_{th} = -866$ mV).

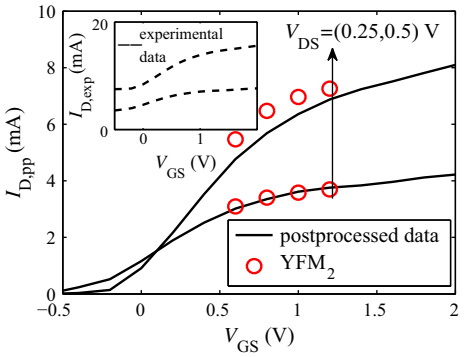

Fig. 7. Transfer characteristics of a MT CNTFET. The inset figure shows the measured transfer characteristic considering s-tubes and m-tubes. Dashed lines: experimental data. Solid lines: post processed data. Circles: I_D calculated with Eq. (3) considering only s-tubes and using $R_{C,Y2} = 63.9\ k\Omega$ and the mean values of the parameters extracted with YFM_2 ($\beta = 124\ mA\ V^{-2}, \theta = 7.4\ V^{-1}$ and $V_{th} = 98$ mV).

specifications of the device and technology can be found in [19,20]). Fig. 6 shows the measured transfer characteristics at $V_{DS} = 0.5$ V and 1 V for this device. YFM_1 delivers a range of values for the contact resistance $R_{C,Y1}$ in between 601 kΩ and 937 kΩ while YFM_2 gives 33.1 kΩ. Since R_{tot} equals 185 kΩ (at $V_{DS} = 0.5$ V, $V_{GS} = -0.2$ V), YFM_1 overestimates the contact resistance considerably leading to a nonphysical negative channel resistance, while the parameters extracted with YFM_2 are validated by the good agreement of the calculated I_D using Eq. (3) with the experimental data as shown in Fig. 6. The high value of R_{ch} of about 152 kΩ could be associated with impurities and defects along the tube. This leads to a high ratio of channel resistance over the contact resistance of 4.5. Similar results have been obtained with the same method for a different measured ST CNTFET in [22].

4.3.2. Multi-tube CNTFET

YFM_2 has also been applied to measurements of a MT CNTFET previously reported in [19]. Its transfer characteristic is shown in the inset of Fig. 7. MT CNTFETs include not only semiconducting (s-) tubes in the channel but also metallic (m-) tubes which do not allow to switch-off the device properly. Applying YFM_2 to the measurements of MT CNTFETs including m-tubes would not be mathematically consistent with the model described by Eq. (3). Therefore a post processing is applied to the experimental data in order to extract the current flowing through the semiconducting tubes only which enables the application of the extraction methodology. For this, the minimum value of the measured drain current $I_{D,exp}$ is subtracted from the corresponding transfer curve obtaining a postprocessed current $I_{D,pp}$. The postprocessed and experimental data are shown in the main plot and in the inset of Fig. 7, respectively. YFM_2 is applied to the postprocessed data in Fig. 7 in the bias region of V_{GS} = 0.6–1.2 V at V_D = 0.25 V and 0.5 V. It delivers a contact resistance value of 63.9 Ω while the total resistance is 83.3 Ω (at $V_{GS} = 0.6$ V, $V_D = 0.25$ V) yielding a channel resistance R_{ch} of about 19.4 Ω and a ratio of the channel resistance over the contact resistance around 0.3. The extracted parameters are validated by calculating the current considering only s-tubes with Eq. (3) as shown in Fig. 7. The absolute values of the extracted contact and channel resistance are smaller for MT CNTFETs than for ST CNTFETs since several tubes in parallel diminish the total resistance. For the studied device, a number of about 2000 s-tubes is assumed which results in a contact resistance per tube of approximately 128 kΩ/tube.

This same MT CNTFET has been modeled using CCAM where a contact resistance of 76 kΩ/tube has been used to obtain a good agreement between CCAM simulation results and experimental data (see Fig. 10 in [19]). The difference between the 128 kΩ/tube extracted for the contact resistance from the postprocessed experimental data and the 76 kΩ/tube used in CCAM is explained as follows. The impact of the Schottky barriers is captured by the current source in the equivalent circuit of CCAM, so the value of the contact resistance included in the equivalent circuit of the model is associated only to the interaction of the metal and the coated portion of the CNT. This separation of physical effects can not be done in experiments, hence the value of contact resistance extracted from the experimental data includes the impact of both interfaces, the metal-coated CNT interface and the coated-uncoated CNT interface, as shown in Fig. 1. Hence, in this case the extracted $R_{C,Y2}$ can only be used as an initial reference value for the compact model but further considerations need to be done in order to obtain a reasonable and justified value for this model parameter.

4.3.3. 50 nm CNTFET

An extensively studied device is the top-gate ST CNTFET presented in [23] with about 50 nm channel length due to its good electrical characteristics (Fig. 1(c) in [23]). The reported contact resistance value in the original publication is about 3.4 kΩ. This has been obtained by fitting a numerical model to the experimental data which does not include the contribution of R_q. The latter has been validated in [24] where the same device has been modeled with a Schrödinger-Poisson solver assuming ballistic transport, as in [23], and in which the contribution of R_q is not included. The electrical characteristics of the device in [23] have been matched by the results obtained in [24].

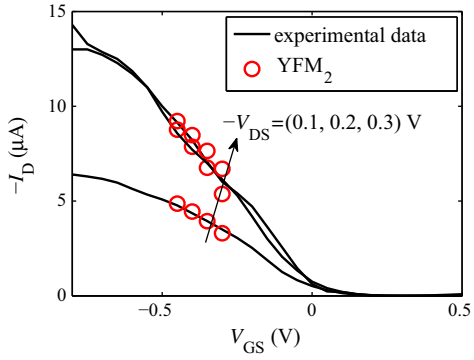

Fig. 8. Measured transfer characteristics of a ST CNTFET previously reported in [23]. Solid lines: experimental data. Circles: I_D calculated with Eq. (3) using $R_{C,Y2} = 9.2\ k\Omega$ and the mean values of the parameters extracted with YFM_2 ($\beta = 272\ \mu AV^{-2}, \theta = 3.17\ V^{-1}$ and $V_{th} = 34.9$ mV).

YFM_2 has been applied to the experimental data taken from [23] in the bias region from V_{GS} = −0.5 V to −0.3 V at V_{DS} = −0.3 V, −0.2 V and −0.1 V. The extracted value of the contact resistance is 9.2 kΩ which includes the contribution of R_q, while the total resistance is about 36 kΩ (at $V_{GS} = -0.3$ V, $V_{DS} = -0.1$ V) yielding a channel resistance R_{ch} of about 26.8 kΩ and a high ratio of $R_{ch}/R_{C,Y2}$ of about 2.9. The validation of the extracted parameters is done by the comparison of the calculated current and the measurements reported in [23] shown here in Fig. 8, obtaining a good agreement in the bias region where the method has been applied. In addition to this, it is worth to notice that if the value of the quantum resistance of 6.5 kΩ is subtracted from the contact resistance value, i.e., $R_{C,Y2} - R_q = 9.2\ k\Omega - 6.5\ k\Omega = 2.7\ k\Omega$, a result that is closer to the reported contact resistance of 3.4 kΩ is obtained.

5. Conclusions

Two different methods based on the Y-function, labeled as YFM_1 and YFM_2, have been applied to extract the value of the contact resistance in single- and multi-tube CNTFETs working within the quasi-ballistic regime or in the diffusive limit. Both methods, developed within the framework of long channel Si MOSFET theory, are physically justified by reinterpreting the traditional MOSFET models for nanoscale devices and can be verified by calculating the drain current with the parameters extracted with each method.

Due to the intrinsic ballistic properties of short CNTs, the ratio of the channel resistance over the contact resistance in sufficiently short CNTFETs is expected to be less than one as it can be seen in the results of the devices simulated with BTE and the measured MT CNTFET. Nevertheless, due to impurities and defects in the fabrication of CNTs, this ratio can be also greater than one. This case has also been shown here for the measured ST CNTFET and the transistor reported in [23]. For the different cases where the YFMs were applied here, YFM_2 turned out to be the most reliable method independently of the actual value of the resistance ratio. The successful application of the latter has been shown here for the first time for CNTFETs.

The methods have been applied to data from a numerical device simulator where it has been found that the contact resistance extracted with YFM_2 is similar to the value extracted from the well-known TLM in the same bias region, implying a similar confidence. However, YFM_2 has the advantage over TLM that no special test structures are needed, making it applicable to single transistors. In addition to this, by increasing the channel length in the numerical device simulations and noticing that even when the total resistance increases, the contact resistance remains almost the same in devices with the same contact characteristics but different channel lengths. Thus, it has been shown that the value extracted with YFM_2 does not include significant contributions from the channel resistance.

The extracted value of contact resistance obtained from the experimental data of a MT CNTFET differs from the value used in the compact model of the corresponding device. Therefore, in order to obtain a valid value for the contact resistance used in a compact model, further studies and methodologies need to be performed which must take into account the corresponding effects described by this model parameter. An statistical approach of the method would be beneficial for the case of MT structures since it could lead to a more physics based modeling of contact resistance extraction in arrays of carbon nanotubes.

YFM_2 has been applied to a ST CNTFET previously published in [23] obtaining a contact resistance value similar to the one reported in the original publication if the quantum resistance is subtracted from $R_{C,Y2}$. Further investigations need to be carried out in order to obtain a clear understanding of the physical origin of the contact resistance.

Acknowledgment

This project is financially supported in part by the German National Science Foundation DFG (CfAED, CL384/2, SCHR695/6) as well as CONACyT Mexico and CAPES 88881.030371/2013-01.

References

[1] Nougaret L, Happy H, Dambrine G, Derycke V, Bourgoin JP, Green AA, et al. 80 GHz field-effect transistors produced using high purity semiconducting single-walled carbon nanotubes. Appl Phys Lett 2009;94:243505.
[2] Schröter M, Claus M, Sakalas P, Haferlach M, Wang D. Carbon nanotube FET technology for radio-frequency electronics: state-of-the-art overview. IEEE J Electr Dev Soc 2013;1(1):9–20.
[3] Alam A, Rogers C, Paydavosi N, Holland K, Ahmed S, Vaidyanathan M. RF linearity potential of carbon-nanotube transistors versus MOSFETs. IEEE Trans Nanotechnol 2013;12(3):340–51.
[4] Mothes S, Claus M, Schröter M. Towards linearity in Schottky-barrier CNTFETs. IEEE Trans Nanotechnol 2015;14(2):372–8.
[5] Baumgardner JE, Pesetski AA, Murduck JM, Przybysz JX, Adam JD, Zhang H. Inherent linearity in carbon nanotube field-effect transistors. Appl Phys Lett 2007;91(5).
[6] Koswatta S, Valdes-Garcia A, Steiner M, Lin Y-M, Avouris P. Ultimate RF performance potential of carbon electronics. IEEE Trans Microwave Theory Tech 2011;59(10):2739–50.
[7] Franklin A, Chen Z. Length scaling of carbon nanotube transistors. Nat Nanotechnol 2010;5:858–62.
[8] Franklin A, Farmer D, Haensch W. Defining and overcoming the contact resistance challenge in scaled carbon nanotube transistors. ACS Nano 2014;8(7):7333–9.
[9] Knoch J, Appenzeller J. Tunneling phenomena in carbon nanotube field-effect transistors. Phys Status Solidi (a) 2008;205(4):679–94.
[10] Claus M, Mothes S, Blawid S, Schröter M. COOS: a wave-function based Schrödinger-Poisson solver for ballistic nanotube transistors. J Comput Electron 2014. http://dx.doi.org/10.1007/s10825-014-0588-6.
[11] Claus M, Fediai A, Mothes S, Knoch J, Ryndyk D, Blawid S, et al. Towards a multiscale modeling framework for metal-CNT interfaces. Proc IWCE, Paris, vol. 2. p. 1–3.
[12] Schroder D. Semiconductor material and device characterization. Wiley-IEEE Press; 2006.
[13] Ghibaudo G. New method for the extraction of MOSFET parameters. Electron Lett 1988;24(9):543–5.
[14] Cao Q, Han SJ, Tulevski G, Franklin A, Haensch W. Evaluation of field-effect mobility and contact resistance of transistors that use solution processed single walled carbon nanotubes. ACS Nano 2012;6(7):6471–7.
[15] Choi SJ, Benett P, Takei K, Wuang C, Lo C Chi, Javey A, et al. Short-channel transistors constructed with solution-processed carbon nanotubes. ACS Nano 2013;7(1):798–803.
[16] Karsenty A, Chelly A. Application, modeling and limitations of Y-function based methods for massive series resistance in nanoscale SOI MOSFETs. Solid-State Electron 2014;92:12–9.
[17] Lundstrom M, Antoniadis D. Compact models and the physics of nanoscale FETs. IEEE Trans Electr Dev 2014;61(2):225–33.
[18] Schröter M, Haferlach M, Claus M. CCAM compact carbon nanotube field-effect transistor model. NanoHUB 2015. http://dx.doi.org/10.4231/D34F1MK28.
[19] Schröter M, Haferlach M, Pacheco-Sanchez A, Mothes S, Sakalas P, Claus M. A semiphysical large-signal compact carbon nanotube FET model for analog RF applications. IEEE Trans Electr Dev 2015;62(1):52–60.
[20] Schröter M, Kolev P, Wang D, Lin S, Samarakone N, Bronikowski M, et al. A 4 wafer photostepperbased carbon nanotube FET technology for RF applications. In: IEEE MTT-S international microwave symposium.
[21] Claus M, Mothes S, Schröter M. Impact of charge injection limitation on the electrical characteristics of Schottky barrier CNTFETs. In: Proc int semiconductor conf Dresden-Grenoble (ISCDG).
[22] Pacheco-Sanchez A, Mothes S, Claus M, Schröter M. Contact resistance extraction methods for CNTFETs. In: 45th European solid-state device conference (ESSDERC). p. 298–301.
[23] Javey A, Guo J, Farmer DB, Wang Q, Yenilmez E, Gordon RG, et al. Self-aligned ballistic molecular transistors and electrically parallel nanotube arrays. Nano Lett 2004;4(7):1319–22.
[24] Claus M, Mothes S, Blawid S, Schröter M. COOS – a wave-function based Schrödinger-Poisson solver for ballistic nanotube transistors. J Comput Electron 2014. http://dx.doi.org/10.1007/s10825-014-0588-6.